

C-arm Cone-beam CT: General Principles and Technical Considerations for Use in Interventional Radiology

Robert C. Orth, MD, PhD, Michael J. Wallace, MD, and Michael D. Kuo, MD for the Technology Assessment Committee of the Society of Interventional Radiology

Digital flat-panel detector cone-beam computed tomography (CBCT) has recently been adapted for use with C-arm systems. This configuration provides projection radiography, fluoroscopy, digital subtraction angiography, and volumetric computed tomography (CT) capabilities in a single patient setup, within the interventional suite. Such capabilities allow the interventionalist to perform intraprocedural volumetric imaging without the need for patient transportation. Proper use of this new technology requires an understanding of both its capabilities and limitations. This article provides an overview of C-arm CBCT with particular attention to trade-offs between C-arm CBCT systems and conventional multi-detector CT.

J Vasc Interv Radiol 2009; 20:S538–S544

INTRODUCTION

THE interventional radiology suite has historically used two-dimensional radiographic imaging techniques such as digital subtraction angiography (DSA) and standard fluoroscopy to visualize, manipulate, and intervene on three-dimensional (3D) structures. Advances in angiographic interventions, including vascular stent and stent graft placement, thrombolysis, transcatheter embolization, and targeted intravascular oncologic procedures, have

increased the need for accurate 3D characterization of vessels and adjacent structures. Nonangiographic procedures such as percutaneous drain and stent placement and radiofrequency ablation frequently involve complex anatomical relationships, which are difficult to characterize fluoroscopically. In most, if not all of these cases, correlation with cross-sectional imaging is necessary. This often requires generation of pre- and post-intervention computed tomographic (CT) image sets. For procedures requiring real-time 3D imaging for which ultrasound localization is not feasible, intraprocedure CT guidance becomes necessary.

Cross-sectional imaging is a frequently used tool in most interventional radiology departments with CT-guided biopsies and percutaneous drain placements commonly performed procedures. However, these procedures are usually performed outside the interventional suite, thereby limiting access to commonly used interventional equipment while at the same time significantly impacting the diagnostic CT workflow. In busy radiology departments, this can decrease patient throughput where procedural complications

can lead to significant scheduling conflicts. In certain types of interventions, there are situations in which both cross-sectional imaging and real time fluoroscopy are required.

Efforts to develop a robust system for generating 3D data sets suitable for use in interventional and surgical suites led to the development of several novel technologies. Made possible by advances in post-processing algorithms, computed rotational 3D DSA became the first 3D in-suite interventional technique, allowing 3D renderings of digitally subtracted contrast-enhanced vessels. With this technology, multiple DSA images at various projection angles are generated by rotating a conventional angiography unit around the patient. Three-dimensional image sets are generated using a cone-beam backprojection reconstruction algorithm (1–3). Following shortly thereafter, 3D digital angiography was developed, allowing 3D visualization of high-contrast structures including osseous structures and contrast-enhanced vessels. In the case of vascular imaging, 3D digital angiography uses unsubtracted rotational images. Three-dimensional digital angiography has the potential advantage over 3D DSA of no misregistration artifacts

From the Department of Radiology, (R.C.O., M.D.K.) and the Center for Translational Medical Systems (M.D.K.), University of California San Diego Medical Center, 200 W Arbor Dr, San Diego, CA 92103; and the Department of Radiology, The University of Texas M.D. Anderson Cancer Center, Houston, Texas (M.J.W.). Received December 22, 2007; final revision received and accepted February 11, 2008. Address correspondence to M.D.K.; E-mail: mkuo@ucsd.edu

M.J.W. received an honorarium for speaking and grant support from Siemens Medical Solutions, Malvern, Pennsylvania.

This article first appeared in J Vasc Interv Radiol 2008; 19:814–820.

© SIR, 2009

DOI: 10.1016/j.jvir.2009.04.026



Figure 1. Commercial C-arm-mounted flat-panel detector cone-beam CT system. (Available in color online at www.jvir.org.)

and lower patient dose (4). However, detectability of low contrast structures is still limited. In an attempt to overcome the limitation of poor low-contrast visibility, the angio-CT system was developed, which fuses a conventional angiographic system with a fan-beam CT scanner. The patient remains stationary, and a CT scanner on rails is rolled into position as needed. However, this system was expensive and required a large physical space (5).

In the late 90's, experimental systems were developed using cone-beam computed tomography (CBCT). Cone-beam CT research had been ongoing for over a decade in areas such as nuclear medicine and industrial testing before significant interest in diagnostic CT applications developed. Cone-beam CT enables generation of an entire volumetric data set in a single gantry rotation by using a two-dimensional detector system rather than a one-dimensional detector or series of one-dimensional detectors as used in conventional CT (6).

Cone-beam CT mounted on a C-arm was originally performed using an image intensifier system over 20 years

ago (7). However, image intensifier systems and charged couple devices suffer from limited spatial resolution. This led to the development of flat-panel detectors, which provide significantly increased contrast and spatial resolution compared to image intensifier detectors (8). The increased spatial resolution of flat-panel detectors has been demonstrated experimentally using a flat-panel detector system with significantly fewer pixels (970 x 768) than are available with today's systems (9). Furthermore, CBCT is reported to result in decreased radiation and intravenous contrast doses compared to angio-CT in head and neck applications (10).

A number of terms have emerged in the literature to describe these new volumetric imaging technologies, including C-arm CT, cone-beam CT, cone-beam volume CT, volume CT, angiographic CT, and flat-panel CT. In this article, the term *C-arm CBCT* will be used to refer to C-arm-mounted cone-beam CT units employing a digital flat-panel detector. Because all commercially available C-arm CBCT units employ digital flat-

panel detectors, the flat-panel detector term will not be explicitly stated. A number of the issues discussed in this article refer to properties of CBCT in general, whether mounted on a traditional CT gantry or on a C-arm. In these cases, the more generic term *CBCT* will be used, again with the understanding that the detectors are digital flat-panel detectors.

C-arm CBCT allows volumetric data acquisition in a single rotation of the source and detector. A photograph of a commercially available unit is shown in **Figure 1**. This setup is ideally suited for imaging in the interventional suite for several reasons. The system is compact enough to allow mounting on a moving C-arm, thereby allowing the patient to remain stationary during the examination. In a single orbit about the patient, a complete volumetric dataset covering a large anatomic region of interest is generated from which sub-millimeter isotropic reconstructions can be created. The high efficiency two-dimensional detector allows excellent low-contrast detectability, a capability not present on image intensifier detector-based 3D-angiographic systems.

The applications of in-suite 3D imaging are many. For the neurointerventionalist, utility has been demonstrated in intra- and extracranial arteriography, particularly for aneurysm characterization (1–3). Recent investigations suggest that current generation C-arm CBCT systems should be able to reliably discriminate the 40 Hounsfield Units necessary to detect intracranial hemorrhage (11). For characterization of intra- and extracranial stent placement in which the low profile, highly flexible stents lead to minimal radiopacity, C-arm CBCT demonstrated residual stent narrowing and calcified plaque that was not visualized by either projection radiography or DSA (12). C-arm CBCT has also demonstrated utility in the repair of endoleak following endovascular repair of abdominal aortic aneurysms (13). Limited studies using C-arm CBCT for transjugular intrahepatic portosystemic shunt placement and transcatheter arterial embolization are encouraging (14,15).

Outside interventional radiology, clinical studies have been performed and are ongoing to investigate the use of CBCT for brachytherapy and external beam radiotherapy, as well

as for surgical planning in orthopedic, thoracic, abdominal, head and neck, and neurosurgical procedures (16–18). Preclinical investigations suggest that with continued refinement of CBCT imaging, dedicated systems for use in routine diagnostic CT may someday become feasible (19,20).

This article provides an introduction to C-arm CBCT systems utilizing high spatial resolution flat-panel detectors, which in a single compact unit provide the interventionalist with the ability to generate projection radiographic, fluoroscopic, DSA, and CT data sets on a stationary patient. This article focuses on comparisons with standard diagnostic multidetector CT, as successful implementation of C-arm CBCT systems is predicated on the ability to provide diagnostic cross-sectional images, which while perhaps not equivalent in quality to diagnostic multidetector CT images, provide adequate image quality to answer the relevant clinical question while offering the advantage of in-suite 3D imaging.

SYSTEM OVERVIEW

Cone-beam versus Fan-beam Geometries

The central difference between conventional multidetector CT (fan-beam) and CBCT is that CBCT acquires information using a high-resolution two-dimensional detector instead of multiple one-dimensional (1D) detector elements. In standard multidetector CT, a series of detector element rows is used. Illustrations demonstrating cone-beam and fan-beam geometries are shown in **Figures 2 and 3**.

In multi-detector spiral CT, the patient is scanned in a helical fashion with gantry speeds on the order of 0.4 seconds for current state-of-the-art 64-slice scanners. With a detector row width of 0.5–0.6 mm, coverage of approximately 4 cm in the z-axis allows large anatomical regions to be imaged in several seconds. For C-arm CBCT systems, current detector arrays are 40 x 30 cm², allowing 25 x 25 x 18 cm³ volumetric datasets to be generated in a single rotation of the source and detector. However, C-arm CBCT systems currently available require 5–20 seconds for image acquisition. Therefore, despite the fact that multidetector CT

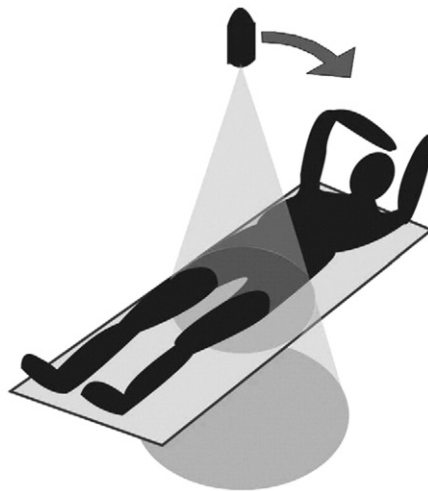


Figure 2. Illustration of cone-beam geometry.

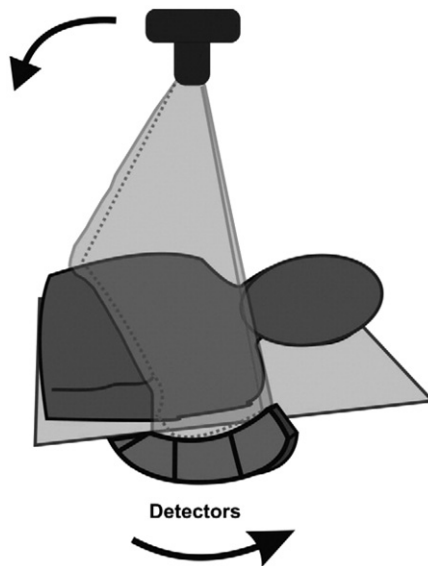


Figure 3. Illustration of fan-beam geometry.

systems require multiple rotations of the CT gantry to cover the same region of interest covered by the C-arm CBCT system in a single rotation, the multidetector CT image acquisition is actually more rapid. Furthermore, due to the mathematical complexity of the cone-beam reconstruction algorithm, which is a modification of the algorithm initially described by Feldkamp (7), state-of-the-art C-arm CBCT systems require 1 minute of post-processing time for image reconstruction, compared to essentially real-time image reconstruction for multidetector CT.

With 2048 x 1538 detector elements, isotropic voxel sizes of under 200 x 200 x 200 μm³ are achievable with current C-arm CBCT systems. Assuming an isotropic voxel size of 600 x 600 x 600 μm³ for current state-of-the-art 64-slice scanners, the flat-panel detector system can theoretically achieve a volumetric resolution reduction factor of approximately 25. However, patient dose considerations make utilization of this high resolution impractical (and unnecessary) for most imaging applications. Furthermore, previous investigations suggest that spatial resolution and noise for the flat-panel detector-based system is governed primarily by blur in the x-ray converter (CsI:Tl) (and reconstruction filter), rather than pixel size, limiting the practical voxel size of current C-arm CBCT systems (21). Therefore, although the pixel size in flat-panel detectors theoretically allows for voxel sizes of 0.008 mm³, blur caused by the x-ray converter and reconstruction filter, protracted reconstruction times, patient dose considerations, and general lack of clinical necessity result in practical C-arm CBCT spatial resolutions similar to, if not slightly larger than, those of multidetector CT.

The most significant difference between 3D tomographic datasets generated via a cone-beam geometry versus a fan-beam geometry is the significant increase in scattered radiation with CBCT (22). In fact, as multidetector CT systems employ increasing numbers of detectors, the geometry changes from fan-beam to cone-beam. The exact point at which this transition occurs is not well defined. Investigations of 256-detector multidetector CT systems, employing cone-beam geometry, demonstrate image quality degradation secondary to scatter similar to that seen with CBCT systems. However, as shown in **Figure 4**, multi-detector CT scanners employ anti-scatter septae between the individual detector channels. Anti-scatter septae of this nature cannot be used with flat-panel detectors. The important point is that increased scatter radiation due to wider x-ray beam collimation in CBCT leads to a significant degradation of image quality. To account for the increased scatter, multiple antiscatter techniques have been investigated for use with CBCT systems including, anti-scatter grids, software correction

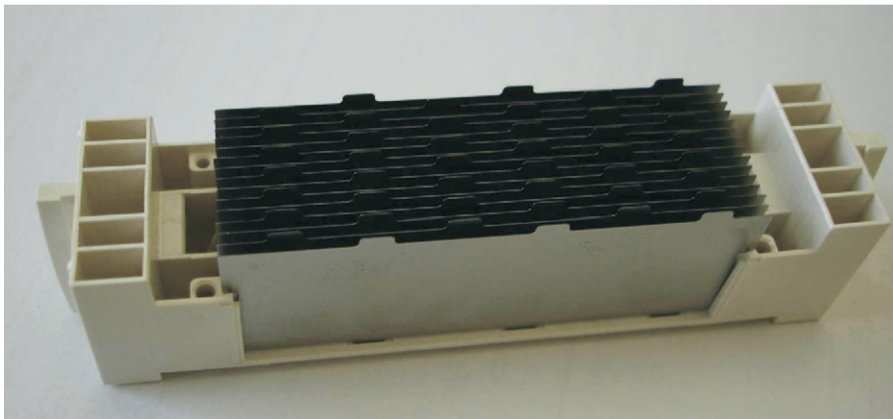


Figure 4. Anti-scatter septae for a multi-detector CT ceramic detector. (Available in color online at www.jvir.org.)

Representative Flat-panel Detector Properties	
Scintillator	CsI:Tl – 600 μm thickness
Photodiodes	2048 \times 1536 (40 \times 30 cm^2) active matrix of a-Si:H and thin film transistors
Pixel pitch	194 μm
Readout speed	15 fps at full resolution and 30 fps at half-resolution (1024 \times 768 at 388 μm pitch)

algorithms, beam-stop scatter mapping, and adjustment of object-to-detector distance (air-gap) (23). These are discussed in detail in the Technical Limitations and Challenges section.

Flat-panel Detector

The **Table** shows representative characteristics for current state-of-the-art flat-panel detectors. Vendors typically offer several gain and effective dynamic range settings, that vary from vendor to vendor. The limitation of 15 frames-per-second (fps) at full resolution is due to the intrinsic properties of the CsI scintillator, which suffers from greater lag (afterglow) compared to multidetector CT ceramic detectors (19). This sets a lower limit on scan time of approximately 3 seconds, with the current fastest C-arm CBCT acquisitions limited to approximately 5 seconds. A photograph of a flat-panel detector is shown in **Figure 5**.

C-arm Unit

In contrast to helical CT, in which the patient is advanced through the scanner with the x-ray source and detector continuously rotating about

the gantry, a C-arm CBCT system generates a complete volumetric dataset with the patient stationary via a single 200° (180° plus fan angle) rotation of the x-ray source and detector. Choice of x-ray tube position during this rotation has implications on the dose to critical patient structures (the eyes in head scanning), which is discussed further below.

TECHNICAL LIMITATIONS AND CHALLENGES

The increased scatter generated by CBCT systems compared to conventional multidetector CT accounts for the most significant differences in image quality between the two systems, resulting in image artifacts, decreased contrast-to-noise (CNR), and inaccuracies in CT number calculations (19). The majority of the following discussion deals with the consequences of scatter on image quality and strategies to mitigate these effects. Differences in dynamic range and temporal resolution between C-arm CBCT and multi-detector CT and the resultant effect on image quality are also discussed.

Causes of Scatter in CBCT

Multidetector helical CT scanners employ multiple rows of detector elements, 64 channels for current systems, with recently introduced models employing 256 and even 320 channels. For current commercial 64-slice systems, the total slab thickness in the z-direction is 4 cm, compared to up to 18 cm for C-arm CBCT systems. For C-arm CBCT systems, this significantly increased imaging volume results in a marked increase in scattered radiation, described by the scatter-to-primary ratio, which is the ratio of scattered to primary radiation incident on the detector. The scatter-to-primary ratio, which is typically around 0.2 for multidetector CT, may increase to greater than 3 for large volume CBCT (24). This results in increased cup and streak artifacts as well as inaccuracies in calculated CT numbers (22). For tomographic images obtained during interventional procedures, the importance of inaccurate CT numbers is not expected to be great. Streak and cupping artifacts, on the other hand, directly impact image quality.

For C-arm CBCT systems, scatter is determined primarily by field-of-view in the z-direction, imaging geometry (which determines the air-gap size), and object size (25). Object size is not an adjustable variable, and while important as larger objects generate greater scatter, will not be discussed further. Air-gaps, which are further discussed below with anti-scatter grids, are not an operator variable and depend on the region of interest and patient size, typically varying from 25 to 35 cm. Field-of-view in the z-direction is the most important adjustable variable for determining scatter magnitude.

As the cone angle is increased to allow larger regions of interest to be imaged, the scatter-to-primary ratio increases significantly. This effect was shown experimentally to increase the scatter-to-primary ratio from 14% for a cone angle of $\sim 0.5^\circ$ to greater than 120% for cone angles greater than 7° . Furthermore, as the cone angle is increased, the scatter fluence at the center of the image plane increases relative to the periphery due to increasing scatter contribution from out-of-plane (22). The cone angle has also been shown experimentally to affect the



Figure 5. Flat-panel CsI *a*-Si:H detector.

presence and magnitude of cupping artifact, which is due to a combination of scattered radiation and beam hardening (19). The cupping artifact, or concave-downward shape of the scatter fluence profile, is decreased with decreasing cone angle and can, for small cone angles, actually be reversed, resulting in a concave upward shape (capping).

The cupping artifact (reduced voxel values near the center of an image), was shown experimentally to increase from approximately 2% for scatter-to-primary ratios of $\sim 10\%$ to almost 20% for scatter-to-primary ratios $\sim 100\%$. Similar inaccuracies were demonstrated for CT numbers, which are underestimated by more than 30% for scatter-to-primary ratios of $\sim 100\%$. Scatter-to-primary ratio values of 100% are expected for abdominal and pelvic imaging (22). For geometries resulting in high scatter-to-primary ratios, detector exposure will increase, thereby reducing voxel noise. However, the decrease in voxel noise is more than offset by the decrease in contrast resulting from the scattered radiation, the end result of which is a decrease in contrast-to-noise with increasing scatter-to-primary ratios. Siewerdsen et al. showed a factor-of-two CNR decrease for scatter-to-primary ratios increased from 0% to 100% (22). As is the case for all radiographic imaging applications, increasing radiation dose or decreasing spatial resolution will increase CNR.

Potential Solution to the Increased Scatter in CBCT

Anti-scatter grids.—Anti-scatter grids and air gaps are employed to eliminate contributions from scattered radiation to the final image. Anti-scatter grids have been shown experimentally to reduce cupping artifact, thereby improving image uniformity with resultant increased CT number accuracy and display dynamic range. Gupta et al. describe measurements showing 80% transmission of primary radiation and 85% reduction in scatter using anti-scatter grids.

For digital detectors, Neitzel showed that air gaps are superior to grids for low scatter situations and that air gaps and scatter grids are nearly equivalent for high scatter conditions. Furthermore, it was shown that for very low scatter situations, the use of a grid actually decreased the signal-to-noise (SNR) secondary to attenuation of the primary beam (26). Siewerdsen et al. showed that for low scatter-to-primary ratio situations where cupping artifact is slight, the increase in noise resulting from the use of an anti-scatter grid causes a decrease in CNR (25). This decrease in CNR may outweigh benefits gained from reduction in the small cupping artifact for these low scatter-to-primary ratio situations. For higher scatter-to-primary ratios, with either high dose or low spatial resolution (input-quantum limited conditions), image quality gains were demonstrated through a significant reduction in the

strong cupping artifact, which outweighed image degradation due to decreased CNR (25). This would be the case when soft-tissue discrimination is favored over high spatial resolution.

The use of anti-scatter grids is a topic not without controversy in the literature, and somewhat similar to its use in fluoroscopy, a blanket statement as to whether or not grids should be used cannot be made. The use of grids leads to a significant increase in patient dose. Removal of the grid from fluoroscopy units has been shown to result in a 65% entrance exposure reduction (27). Current commercial C-arm CBCT systems employ anti-scatter grids, with one manufacturer employing a laminar grid with grid ratio of 15, 80 line-pairs/cm. Because low-scatter situations are unlikely to be encountered clinically with significant regularity, routine employment of an anti-scatter grid is the current standard despite the trade-off of increased patient dose.

One concern when using anti-scatter grids in tomographic imaging is the introduction of ring or line artifacts. Experimental results have shown, however, that 3D reconstructions with CBCT systems suffer very little from ring artifacts. One hypothesis for this result is that geometric calibrations to correct for gantry motion are imperfect, not to the point of reducing image quality, but large enough to blur grid-lines during backprojection. This is analogous to the manner in which motion-bucky blurs the gridlines in projection systems (25). Of note, "Bucky" systems are not currently used in C-arm CBCT systems.

Scatter reduction algorithms.—Elimination of scatter-related image degradation can be partially addressed through the use of scatter correction algorithms (19,24,28). Discussion of these algorithms is beyond the scope of this article. However, development and optimization of scatter correction algorithms is an area of active research and some sort of computational anti-scatter post-processing is performed on all clinical C-arm CBCT systems.

Bowtie filters.—Shaped filters, usually in the form of a bowtie filter, may be used to decrease the scatter contribution from the object periphery and have been shown experimentally to result in improved image quality for gantry-based CBCT systems (19). How-

ever, Ning et al. showed experimentally that $\text{SNR}^2/\text{entrance exposure}$ for a flat-panel-based cone-beam decreases with increasing kVp (8). Therefore, the decision to use a bowtie filter comes down to a tradeoff between decreased scatter from the object periphery with the filter and improved detector efficiency from the softer x-ray beam without the filter. Further evidence to caution against the use of bowtie filters in CBCT systems was provided by Fahrig et al. who investigated the effect of kVp on low contrast detectability, and showed the greatest enhancement at the lowest setting, 70 kVp (11).

Temporal Resolution and Dynamic Range

As mentioned above, flat panel detectors typically use CsI as the scintillator, which has a slower response than the proprietary ceramic detectors used in helical multidetector CT systems. Also, the quantum efficiency of CsI flat-panel detectors is slightly lower. These two characteristics limit the temporal resolution and dynamic range, respectively, of flat-panel detectors compared to standard multidetector CT detectors. Investigations using flat-panel detector systems have shown loss of low-contrast resolution due to streak artifacts caused by a limited number of rotational projections. This is largely the result of the limited temporal resolution of the CsI detectors. Akpek et al. showed that streak artifact remains a significant cause of image quality degradation using 273 projections, thereby limiting contrast resolution (29). These streak artifacts, however, are not of significant importance when high-contrast structures are imaged, such as during arteriographic procedures (5).

For these and other reasons, gantry-mounted CBCT systems are unlikely to substantially challenge the role of helical multi-detector CT in routine diagnostic imaging, at least in the foreseeable future. This is particularly true as multidetector units continue to evolve, with the newest systems now employing cone beam geometries and true volumetric imaging. However, the purpose of C-arm CBCT is not to replace 64-slice helical CT, but rather to bring tomographic imaging with

reasonable low contrast detectability into the interventional suite.

The low-contrast detectability of CsI flat-panel detectors was investigated by Gupta et al. and found to be 5 Hounsfield Units (HU) above background, slightly less than that detectable by multi-detector CT, which can detect objects 3 HU above background. This difference is due to a combination of increased scatter and the lower dynamic range of CsI detectors (19). Nevertheless, this represents a dramatic improvement over the low-contrast detectability of CTangio systems and is, therefore, a significant advancement.

Motion

Because of the relatively long acquisition times of C-arm CBCT systems compared to multislice helical CT, motion artifacts can arise. This is particularly true given the patient population typically undergoing interventional radiology procedures. Algorithms to correct for these artifacts using retrospective respiratory gating are under development (30). With retrospective gating, however, patient dose, which is already an issue of concern in C-arm CBCT, increases.

Mechanical Stability

The magnitude of C-arm flex is several millimeters in the tube and detector components and increases when the system is angulated (up to ~14 mm in projection space at 45°). However, because the C-arm flex is reproducible, even at steep angulations, as long as appropriate geometric calibrations are performed, precise 3D reconstructions are possible (21).

Radiation Dose

The issue of patient dose in C-arm CBCT is complex. First, comparisons with multidetector CT are complicated by lack of a universally accepted common dose metric. CT dose index (CTDI) and the dose length product (DLP) do not correctly apply to cone beam geometries secondary to the large z-coverage of a flat panel detector. Also, the dose is non-linear with the central slice getting the highest dose (19). Second, direct comparisons in the literature are limited by lack of

equivalent image quality in the resultant image sets. Through a 200 degree rotation of the gantry, the C-arm CBCT system generates tomographic data sets that have been shown experimentally to result in patient doses less than that from single helical CT (5). However, it was noted in this experiment that spatial and contrast resolution of the flat-panel detector system is inferior to that obtained with multidetector CT. This is due in large part to a lack of filtration and scatter rejection with the C-arm CBCT system, which in turn results in decreased SNR. Similar findings were described by Gupta et al. for comparisons between a gantry-mounted flat-panel system and 16-slice multidetector CT (19). Finally, because C-arm CBCT operates with automatic exposure control systems controlling the mA, and if necessary, the kVp to maintain SNR, control of patient dose in C-arm CBCT systems is more difficult.

Unlike multidetector CT, in which the collimation is fixed, careful consideration must be taken with CBCT to limit the imaging field-of-view to the anatomical area of interest. This will decrease total radiation resulting in lower patient dose and improved image contrast through a reduction in scattered radiation.

Consideration of tube position can affect the dose to sensitive structures for anisotropic regions-of-interest such as with head CT scans. Daly et al. showed a factor of 5 decrease in dose to the eyes when CT images were generated with a 178° imaging arc performed with the x-ray tube posterior to the skull rather than anterior. In addition, because attenuation by the table takes place prior to irradiation of the patient's head, image quality per unit patient dose is improved (16).

In general, the effect of C-arm CBCT on overall patient dose remains to be seen. On the one hand, judicious use of in-suite CBCT may actually result in a decrease in patient dose by providing critical diagnostic information that obviates the need for excessive fluoroscopy. Alternatively, the simple availability of this technique may lead to overuse and increased patient radiation. An investigation into CBCT for use in minimally invasive spine surgery by Siewerdsen et al. showed anecdotally that "the surgeon exhibited a gravitation toward the use of intra-operative 3D imaging guidance" over the course of several surger-

ies (21). Although this trend may not affect interventional radiologists to the same extent, it raises an interesting concern given the potential for escalating patient doses. Further investigations into physician practice patterns and patient dosimetry are needed to better address these questions.

CONCLUSION

In this article, the main cause of image quality degradation with C-arm CBCT, increased scatter radiation, was discussed along with several strategies for scatter reduction and compensation. Many of the scatter reduction strategies discussed are outside the control of the operating physician. Imaging volume, however, is within the operating physician's control and is the largest single factor determining the amount of scattered radiation. Furthermore, for a given set of imaging parameters, imaging volume determines patient dose. The field-of-view should be kept as small as possible to minimize both the scatter-to-primary ratio and patient dose.

C-arm CBCT is an exciting technology with the potential to significantly impact the practice of interventional radiology. The ability to perform near real-time 3D imaging in the interventional suite will directly affect patient care while increasing overall radiology department efficiency by allowing all interventional procedures, CT-guided or otherwise, to be performed in the interventional suite. However, because this is a new technology, much remains to be determined, from practice guidelines to the impact on overall patient radiation dose.

References

- Hochmuth A, Spetzger U, Schumacher M. Comparison of three-dimensional rotational angiography with digital subtraction angiography in the assessment of ruptured cerebral aneurysms. *AJNR* 2002; 23:1199–1205.
- Missler U, Hundt C, Wiesmann M, Mayer T, Bruckmann H. Three-dimensional reconstructed rotational digital subtraction angiography in planning treatment of intracranial aneurysms. *European Radiology* 2000; 10: 564–568.
- Song JK, Niimi Y, Brisman JL, Berenstein A. Simultaneous bilateral internal carotid artery 3D rotational angiography. *AJNR* 2004; 25:1787–1789.
- Hirai T, Korogi Y, Suginozawa K, et al. Clinical usefulness of unsubtracted 3D digital angiography compared with rotational digital angiography in the pre-treatment evaluation of intracranial aneurysms. *AJNR* 2003; 24:1067–1074.
- Hirota S, Nakao N, Yamamoto S, et al. Cone-beam CT with flat-panel-detector digital angiography system: early experience in abdominal interventional procedures. *Cardiovasc Intervent Radiol* 2006; 29:1034–1038.
- Jaffray DA, Siewerdsen JH. Cone-beam computed tomography with a flat-panel imager: initial performance characterization. *Medical Physics* 2000; 27: 1311–1323.
- Feldkamp LA, Davis LC, Kress JW. Practical cone-beam algorithm. *J Opt Soc Amer* 1984; 1:612–619.
- Ning R, Chen B, Yu R, Conover D, Tang X, Ning Y. Flat panel detector-based cone-beam volume CT angiography imaging: system evaluation. *IEEE Transactions on Medical Imaging* 2000; 19:949–963.
- Baba R, Konno Y, Ueda K, Ikeda S. Comparison of flat-panel detector and image-intensifier detector for cone-beam CT. *Comput Med Imaging Graph* 2002; 26:153–158.
- Ishikura R, Ando K, Nagami Y, et al. Evaluation of vascular supply with cone-beam computed tomography during intraarterial chemotherapy for a skull base tumor. *Radiat Med* 2006; 24:384–387.
- Fahrig R, Dixon R, Payne T, Morin RL, Ganguly A, Strobel N. Dose and image quality for a cone-beam C-arm CT system. *Medical Physics* 2006; 33:4541–4550.
- Benndorf G, Strother CM, Claus B, et al. Angiographic CT in cerebrovascular stenting. *AJNR* 2005; 26:1813–1818.
- Binkert CA, Alencar H, Singh J, Baum RA. Translumbar type II endoleak repair using angiographic CT. *J Vasc Interv Radiol* 2006; 17:1349–1353.
- Kakeda S, Korogi Y, Ohnari N, et al. Usefulness of cone-beam volume CT with flat panel detectors in conjunction with catheter angiography for transcatheter arterial embolization. *J Vasc Interv Radiol* 2007; 18:1508–1516.
- Sze DY, Strobel N, Fahrig R, Moore T, Busque S, Frisoli JK. Transjugular intrahepatic portosystemic shunt creation in a polycystic liver facilitated by hybrid cross-sectional/angiographic imaging. *J Vasc Interv Radiol* 2006; 17: 711–715.
- Daly MJ, Siewerdsen JH, Moseley DJ, Jaffray DA, Irish JC. Intraoperative cone-beam CT for guidance of head and neck surgery: Assessment of dose and image quality using a C-arm prototype. *Medical Physics* 2006; 33:3767–3780.
- Jaffray DA, Siewerdsen JH, Wong JW, Martinez AA. Flat-panel cone-beam computed tomography for image-guided radiation therapy. *International Journal of Radiation Oncology, Biology, Physics* 2002; 53:1337–1349.
- Rafferty MA, Siewerdsen JH, Chan Y, et al. Intraoperative cone-beam CT for guidance of temporal bone surgery. *Otolaryngol Head Neck Surg* 2006; 134: 801–808.
- Gupta R, Grasruck M, Suess C, et al. Ultra-high resolution flat-panel volume CT: fundamental principles, design architecture, and system characterization. *European Radiology* 2006; 16:1191–1205.
- Kalender WA. X-ray computed tomography. *Phys Med Biol* 2006; 51: R29–43.
- Siewerdsen JH, Moseley DJ, Burch S, et al. Volume CT with a flat-panel detector on a mobile, isocentric C-arm: pre-clinical investigation in guidance of minimally invasive surgery. *Medical Physics* 2005; 32:241–254.
- Siewerdsen JH, Jaffray DA. Cone-beam computed tomography with a flat-panel imager: magnitude and effects of x-ray scatter. *Medical Physics* 2001; 28: 220–231.
- Endo M, Mori S, Tsunoo T, Miyazaki H. Magnitude and effects of x-ray scatter in a 256-slice CT scanner. *Medical Physics* 2006; 33:3359–3368.
- Ning R, Tang X, Conover D. X-ray scatter correction algorithm for cone beam CT imaging. *Medical Physics* 2004; 31:1195–1202.
- Siewerdsen JH, Moseley DJ, Bakhtiar B, Richard S, Jaffray DA. The influence of antiscatter grids on soft-tissue detectability in cone-beam computed tomography with flat-panel detectors. *Medical Physics* 2004; 31:3506–3520.
- Neitzel U. Grids or air gaps for scatter reduction in digital radiography: a model calculation. *Medical Physics* 1992; 19:475–481.
- Nickoloff EL, Lu ZF, Dutta A, So J, Balter S, Moses J. Influence of flat-panel fluoroscopic equipment variables on cardiac radiation doses. *Cardiovasc Intervent Radiol* 2007; 30:169–176.
- Zellerhoff M, Scholz B, Ruhmschopf E, Brunner T. Low contrast 3D-reconstruction from C-arm data. *Proc Soc Photo Opt Instrum Eng* 2005; 5745: 646–655.
- Akpek S, Brunner T, Benndorf G, Strother C. Three-dimensional imaging and cone beam volume CT in C-arm angiography with flat panel detector. *Diagn Interv Radiol* 2005; 11:10–13.
- Kriminski S, Mitschke M, Sorensen S, et al. Respiratory correlated cone-beam computed tomography on an isocentric C-arm. *Phys Med Biol* 2005; 50: 5263–5280.